$\zeta=0$, $\epsilon=\epsilon_0$, and $\zeta_0=\zeta_{0M}$. We note that Δ here is the solution of the surface-nucleation problem in the GL region which is known to be[4]

$$\Delta(\zeta)=D_{\frac{1}{2}(\epsilon_0-1)}[\sqrt{2}(\zeta-\zeta_0)].$$

Then we have

$$C=-D_{\frac{1}{2}(\epsilon_0-1)}(-\sqrt{2}\zeta_{0M})\Big/\left[\frac{\partial^2 D_{\frac{1}{2}(\epsilon_0-1)}(-\sqrt{2}\zeta_{0M})}{\partial\epsilon_0\partial\zeta_{0M}}\right],$$

which is an intrinsic property of these parabolic cylinder functions. It is this expression which has been evaluated by Schultens.[16,17]

APPENDIX B: EFFECTIVE-BOUNDARY-CONDITION PARAMETER TO THIRD ORDER

To find $\alpha^{(3)}$ we must first evaluate $\mathbf{O}^{\mathrm{SL}}\Delta^B$ to fourth order. A tedious but straightforward expansion of the surface term in Eq. (11) yields[7]

$$\begin{aligned}\mathbf{O}^{\mathrm{SL}}\Delta^B(\mathbf{r})=&\,\mathrm{SLT}(III)+z\chi_{2,1}(z)\mathfrak{D}_\perp{}^2\mathfrak{D}_z{}^2\Delta^B(\mathbf{r})\\&+\tfrac{1}{3}[z^3\chi_1(z)+z\chi_3(z)]\mathfrak{D}_z{}^4\Delta^B(\mathbf{r})\\&+[z^2\chi_{2,1}{}^{(1)}(z)-3z\chi_{2,2}{}^{(1)}(z)]\xi_H{}^{-2}\mathfrak{D}_x\mathfrak{D}_z\Delta^B(\mathbf{r})\\&-[\tfrac{1}{2}z^2\chi_{2,2}{}^{(2)}(z)-z\chi_{2,3}{}^{(2)}(z)]\xi_H{}^{-4}\Delta^B(\mathbf{r}),\end{aligned}$$

where $\mathrm{SLT}(III)$ is defined in Eqs. (13) and (17) while the various χ's are defined by Eqs. (18). Now using Eqs. (19) and (22) and in our special gauge, the above is expanded in a Taylor series around $z=0$ and the term proportional to α separated out to give

$$\begin{aligned}f_1{}^{(2)}(z)=&-2\chi_1(z)\xi_H{}^{-1}\\f_2{}^{(4)}(z)=&[\chi_{2,2}{}^{(1)}(z)+\tfrac{2}{3}\chi_3(z)]\xi_H{}^{-3}\zeta_0\\&+[\tfrac{1}{2}z^2\chi_{2,2}{}^{(2)}(z)-z\chi_{2,3}{}^{(2)}(z)-z\chi_{2,2}{}^{(1)}(z)]\xi_H{}^{-4}.\end{aligned}$$

These may be substituted in Eq. (37) and the integrations performed to finally give Eq. (43).

PHYSICAL REVIEW VOLUME 185, NUMBER 2 10 SEPTEMBER 1969

Alfvén-Wave Propagation in Solid-State Plasmas. III. Quantum Oscillations of the Fermi Surface of Bismuth*†

R. T. Isaacson‡ and G. A. Williams
Department of Physics, The University of Utah, Salt Lake City, Utah 84112
(Received 14 February 1969)

We have measured the quantum oscillations of Alfvén-wave mass densities in pure bismuth. To fit the experimental results, we use a four-energy-band model, corresponding to three equivalent nonparabolic ellipsoidal electron Fermi surfaces and one nonparabolic ellipsoidal hole Fermi surface. This enables us to evaluate the number of carriers, the carrier masses, the two energy gaps, the Fermi energy, and the overlap energy. These experiments yield a value for the energy gap E_{G2} of 250±50 meV. The value of the overlap energy is increased over the previously reported value of 36.0 meV. We find a value of 38.2±0.15 meV necessary. The other numerical parameters used are taken from previous values with some refinement. They are $n=(2.92\pm0.05)\times10^{17}$ cm^{-3}, $m_1=0.00651$, $m_2=1.362$, $m_3=0.0297$, $m_4=\pm0.1635$, $M_1=0.0644$, $M_3=0.696$, $E_F=26.6\pm0.18$ meV, and $E_{G1}=15.0$ meV. In addition, estimates are made for the lattice dielectric constant for several orientations.

I. INTRODUCTION

THE phase velocity of Alfvén waves in solids is determined by two quantities, the strength of the magnetic field and the mass density of the charge carriers. In a classical description the mass density is unaffected by a magnetic field. The quantization of electron energy into Landau levels brought about by a magnetic field causes the Fermi energy to oscillate in value as a function of the magnetic field.[1,2] This oscillation causes the number of carriers and, hence, the mass density also to oscillate with the magnetic field. The deviation of the mass density from its classical value is the subject of this paper.

Buchsbaum and Galt[3] pointed out that Alfvén waves could propagate in certain solid-state plasmas. Since then, Alfvén-wave propagation in bismuth has been

* This work was supported by the U. S. Air force Office of Scientific Research under Grant No. AFOSR 901-65.

† Based in part on a thesis submitted by R. T. Isaacson to the University of Utah in partial fulfillment of the requirements for the degree of Doctor of Philosophy.

‡ NASA Predoctoral Fellow, 1964–1966. Present address: Physics Department, University of Ottawa, Ottawa 2, Ontario, Canada.

[1] G. A. Williams and G. E. Smith, IBM J. Res. Develop. 8, 276 (1964).

[2] G. E. Smith, G. A. Baraff, and J. M. Rowell, Phys. Rev. 135, A1118 (1964).

[3] S. J. Buchsbaum and J. K. Galt, Phys. Fluids 4, 1514 (1961).

studied in several laboratories.[1,4–16] Buchsbaum[17] and Bowers[18] have discussed the theoretical and experimental properties of electromagnetic wave propagation in solid-state plasmas and reviewed the previous literature. It was first pointed out by Williams and Smith[1] that the Alfvén-wave phase velocity was sensitive to the variation in carrier mass density and in the Fermi level. The present work continues the work of Williams and Smith for all orientations of the bismuth crystal. Useful information concerning the lattice dielectric constant, the energy gaps between bands, and the mass densities is obtained.

In Sec. II, the theory of Alfvén-wave propagation in a simple isotropic plasma is presented. The experimental details are discussed in Sec. III. The results and discussion are presented in Sec. IV.

II. THEORY

A. Alfvén-Wave Propagation

Allis, Buchsbaum, and Bers[19] have discussed the detailed theory of the propagation of electromagnetic waves in anisotropic plasmas. We will present a simpler theory,[1,7] based on an isotropic simple plasma and indicate the changes needed for the anisotropic case.

The equation of motion for n carriers of charge e and effective mass m^* in a magnetic field $\mathbf{H}$ is

$$nem^*d\mathbf{v}/dt=ne^2[\mathbf{E}+(\mathbf{v}\times\mathbf{H})/c]-nem^*\mathbf{v}/\tau, \quad (1)$$

where τ is the scattering time. Letting the current be $\mathbf{J}=ne\mathbf{v}$, we can convert Eq. (1) into an expression involving $\mathbf{H}$, $\mathbf{J}$, and $\mathbf{E}$. Assuming $\mathbf{H}$ is along the z axis and that both $\mathbf{J}$ and $\mathbf{E}$ are harmonic with frequency ω, we can solve for $\mathbf{J}$ in terms of $\mathbf{E}$ and $\mathbf{H}$. Since $\mathbf{J}=\boldsymbol{\sigma}\cdot\mathbf{E}$, we can obtain the electrical conductivity $\boldsymbol{\sigma}$ and, thus, the effective dielectric constant.

$$\boldsymbol{\epsilon}_{\text{eff}}=\boldsymbol{\epsilon}_l-(4\pi i/\omega)\boldsymbol{\sigma}, \quad (2)$$

where $\boldsymbol{\epsilon}_l$ is the lattice-dielectric-constant tensor. This contains all contributions to the dielectric constant except that of the charge carriers under discussion. After obtaining $\boldsymbol{\sigma}$ from Eq. (1), and with $\omega_c=eH/m^*c$, Eq. (2) becomes

$$\epsilon_{\text{eff}}=\epsilon_l-\frac{4\pi ine^2\tau/m^*\omega}{1+i(\omega-\omega_c)\tau}. \quad (3)$$

For $|(\omega-\omega_c)\tau|\gg1$ and the plasma frequency ω_p given by $\omega_p^2=4\pi ne^2/m^*$, this expression becomes

$$\epsilon_{\text{eff}}=\epsilon_l+\omega_p^2/\omega(\omega_c-\omega)$$

for a single group of carriers. The effective dielectric constant is written here and in Eq. (3) as a scalar because we have specialized to the case of isotropic effective masses. If there are two kinds of carriers, electrons and holes,

$$\epsilon_{\text{eff}}=\epsilon_l+\frac{\omega_p^2}{\omega(\omega_c-\omega)}+\frac{\Omega_p^2}{\omega(\Omega_c-\omega)}. \quad (4)$$

Here Ω_p and Ω_c are the plasma and cyclotron frequencies, respectively, for the holes.

In these experiments, at attainable magnetic fields, it is always true that $\omega_p>\omega_c$ and $\Omega_p>\Omega_c$. If we chose a microwave frequency ω such that $\omega_c>\omega$ and $\Omega_c>\omega$ for the magnetic fields used, then electromagnetic waves can propagate in the medium, because the total dielectric constant is real and positive. For magnetic fields in which these conditions are satisfied, the denominator of the terms in Eq. (4) can be expanded to yield

$$\epsilon_{\text{eff}}=\epsilon_l+\frac{\omega_p^2}{\omega\omega_c}\left(1+\frac{\omega}{\omega_c}+\cdots\right)+\frac{\Omega_p^2}{\omega\Omega_c}\left(1+\frac{\omega}{\Omega_c}+\cdots\right). \quad (5)$$

When the expressions for ω_p, ω_c, Ω_c, and Ω_p are substituted into Eq. (5), we obtain

$$\epsilon_{\text{eff}}=\epsilon_l+\frac{4\pi ce}{\omega H}(p-n)+\frac{4\pi c^2}{H^2}(nm_e+pm_h)+\cdots, \quad (6)$$

where p and n are the number of holes and electrons, respectively. The second term in Eq. (6) is the helicon term, which vanishes for a compensated material like pure bismuth where $p=n$. We have alloyed bismuth with several parts per million of acceptor impurities, lead and tin, but have not yet seen the effect of the helicon term. The third term is the Alfvén-wave term. For an anisotropic material material such as bismuth the expression $nm_e^*+pm_h^*$ must be replaced by a more complex term $f(nm_e^*+pn_h^*)$ that depends on the direction of the magnetic field with respect to the crystal axes. Despite the complications introduced by anisotropy, the Alfvén-wave effective dielectric constant still

[4] J. Kirsch, Phys. Rev. **133**, A1390 (1964).
[5] M. S. Khaikin, V. S. Edel'man, and R. T. Mina, Zh. Eksperim. i Teor. Fiz. **44**, 2190 (1963) [English transl.: Soviet Phys.—JETP **17**, 1470 (1963)].
[6] M. S. Khaikin, La Fal'kduskii, V. S. Edel'man, and R. T. Mina, Zh. Eksperim. i Teor. Fiz. **45**, 1839 (1963) [English transl.: Soviet Phys.—JETP **18**, 1167 (1964)].
[7] G. A. Williams, Phys. Rev. **139**, A771 (1965).
[8] D. S. McLachlan, Phys. Rev. **147**, 368 (1966).
[9] B. W. Faughnan, J. Phys. Soc. Japan **20**, 574 (1965).
[10] D. S. Bartelink and W. A. Nordland, Phys. Rev. **152**, 556 (1966).
[11] W. L. Lupatkin and C. A. Nanney, Phys. Rev. Letters **20**, 212 (1968).
[12] D. L. Carter and J. C. Picard, Solid State Commun. **5**, 719 (1967).
[13] H. Kawamura, S. Nagata, T. Kanama, and S. Takano, Phys. Letters **15**, 111 (1965).
[14] M. S. Khaikin and V. S. Edel'man, Zh. Eskperim. i Teor. Fiz. **49**, 1965 (1965) [English transl.: Soviet Phys.—JETP **22**, 1159 (1966)].
[15] S. Nagata and H. Kawamura, J. Phys. Soc. Japan **24**, 480 (1968).
[16] R. T. Isaacson and G. A. Williams, Phys. Rev. **177**, 738 (1969).
[17] S. J. Buchsbaum, in *Symposium on Plasma Effects in Solids, Paris 1964* (Academic Press Inc., New York, 1965).
[18] R. Bowers, in *Symposium on Plasma Effects in Solids, Paris 1964* (Academic Press Inc., New York, 1965).
[19] W. P. Allis, S. J. Buchsbaum, and A. Bers, *Waves in Anisotropic Plasmas* (The M. I. T. Press, Cambridge, 1963).

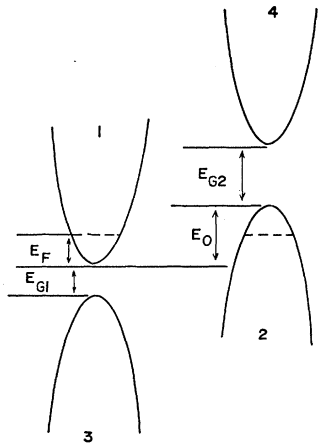

FIG. 1. Model of the bismuth band structure.

depends linearly on $1/H^2$ and is independent of frequency, as in the isotropic case.

B. Quantum Oscillations

The theory given thus far is sufficient to explain the gross features of Alfvén-wave propagation. But to account for the details discussed in this paper we must take into account the quantization of electron energy into Landau levels. This quantization leads to oscillatory effects in the mass density due to the Landau levels crossing the Fermi surface.[20] The de Haas–Shubnikov and de Haas–van Alphen effects are other examples of this type of effect. For magnetic fields in which there are a large number of Landau levels below the Fermi energy, the oscillations are periodic in $1/H$. As the magnetic field is increased the Fermi energy may no longer be considered constant, since it undergoes oscillations. This oscillation of the Fermi level destroys the periodicity of the oscillatory effect. In order to account for these effects, we follow the calculations of Smith, Baraff, and Rowell.[2]

The model of the bismuth Fermi surface used consists of three equivalent electron ellipsoids and a single-hole ellipsoid. The corresponding band structure is shown in Fig. 1. Band 3 is well known and gives rise to the nonparabolicity of the adjacent electron conduction band which was included in the calculations in Ref. 2. Band 4 is added, since its existence has been verified by adding impurity atoms to bismuth to raise the Fermi energy.[21–27] There is some indication that it is close enough to band 2 to cause nonparabolicity in the hole energy band.[21–23] Experimental evidence indicates that any nonellipsoidal shape of the electron Fermi surface is slight.[14,28–31] Alfvén-wave mass densities depend only on the ellipsoidal character of the Fermi surface and the effective-mass components at the Fermi surface. Therefore, measurements of Alfvén-wave velocities alone are not sufficient to distinguish between parabolic and nonparabolic bands.

For one electron ellipsoid in bismuth in the absence of a magnetic field, we have the following nonparabolic relationship between energy and momentum, taking into account the presence of an adjacent band with an energy gap E_G:

$$E(1+E/E_G)=\mathbf{p}\cdot\boldsymbol{\alpha}\cdot\mathbf{p}/2m_0, \tag{7}$$

where $\boldsymbol{\alpha}$ is the inverse effective-mass tensor. In bismuth, one inverse electron-mass tensor is of the form

$$\boldsymbol{\alpha}=\begin{bmatrix}\alpha_1 & 0 & 0\\ 0 & \alpha_2 & \alpha_4\\ 0 & \alpha_4 & \alpha_3\end{bmatrix}, \tag{8}$$

where 1, 2, and 3 refer to the binary, bisectrix, and trigonal axes, respectively. The other two electron ellipsoids are obtained by $\pm 120°$ rotations about the trigonal axis.

For the holes, the energy-momentum relation is taken to be the same as the one for the electrons with an inverse mass tensor of the form

$$\boldsymbol{\beta}=\begin{bmatrix}\beta_1 & 0 & 0\\ 0 & \beta_1 & 0\\ 0 & 0 & \beta_3\end{bmatrix}. \tag{9}$$

The hole Fermi energy is $E_h=E_0-E_F$, where E_0 is the overlap energy of bands 1 and 2 and E_F is the electron Fermi energy. If in Eq. (7) we let $E_G=E_{G1}$, the energy gap between bands 2 and 3, then Eq. (7) describes the electron Fermi-surface ellipsoids. If we set $E_G=E_{G2}$, the gap between bands 1 and 4, and use the mass tensor (9) for the holes, then Eq. (7) will describe the hole Fermi surface. If E_{G2} becomes very large compared to the other energies, then the energy-momentum expression for the holes reduces to its usual parabolic form:

$$E_0-E_F=(1/2m_0)[(p_1^2+p_2^2)\beta_1+p_3^2\beta_3]. \tag{10}$$

The carrier density in each ellipsoid is determined by the Fermi level and is proportional to the volume of momentum space bounded by the Fermi energy surface.

[20] I. M. Lifshitz and A. M. Kosevich, Zh. Eksperim. i Teor. Fiz. **29**, 730 (1955) [English transl.: Sov. Phys.—JETP **2**, 636 (1956)].
[21] G. A. Antcliffe and R. T. Bate, Phys. Rev. **160**, 531 (1967).
[22] R. T. Bate and N. G. Einspruch, Phys. Rev. **153**, 796 (1967).
[23] J. M. Noothoven van Goor, Phys. Letters **25A**, 442 (1967).
[24] Takeshi Morimoto, J. Phys. Soc. Japan **21**, 1008 (1966).
[25] L. Esaki and P. J. Stiles, Phys. Rev. Letters **14**, 902 (1965).
[26] L. Esaki, L. L. Chang, P. J. Stiles, D. F. O'Kane, and Nathan Wiser, Phys. Rev. **167**, 637 (1968).
[27] L. A. Fal'kovskii and G. S. Razina, Zh. Eksperim. i Teor. Fiz. **49**, 265 (1965) [English transl.: Soviet Phys.—JETP **22**, 187 (1966)].
[28] R. N. Bhargava, Phys. Rev. **156**, 785 (1967).
[29] N. B. Brandt, T. F. Dolgolenko, and N. N. Stupuchenko, Zh. Eksperim. i Teor. Fiz. **45**, 1319 (1963) [English transl.: Soviet Phys.—JETP **18**, 908 (1964)].
[30] V. S. Edel'man and M. S. Khaikin, Zh. Eksperim. i Teor. Fiz. **49**, 107 (1965) [English transl.: Soviet Phys.—JETP **22**, 77 (1966)].
[31] A. P. Korolyuk, Zh. Eksperim. i Teor. Fiz. **49**, 1009 (1965) [English Transl.: Soviet Phys.—JETP **22**, 701 (1966)].

The Fermi energy is found by requiring that the number of holes and electrons be equal.

In the presence of a magnetic field, the carrier energies are given by

$$E(1+E/E_G)=(n+\tfrac{1}{2})\hbar\omega_c+p_z^2/2m_0\pm\tfrac{1}{2}g\beta_0H\,,\qquad n=0,\,1,\,2,\cdots,\quad(11)$$

where $\omega_c=eH/m_cc$, and where the longitudinal and cyclotron masses m_z and m_c are

$$m_z=\mathbf{H}\cdot\mathbf{m}\cdot\mathbf{H}/H^2\quad\text{and}\quad m_c=[(\det\mathbf{m}^*)/m_z]^{1/2}.\quad(12)$$

The effective-mass tensor m is given by $\mathbf{m}^*=\boldsymbol{\alpha}^{-1}$. The effective g factor is defined in terms of a spin-mass tensor[2] $\mathbf{m}_s$ by

$$g^2=4m_0^2\mathbf{H}\cdot\mathbf{m}_s\cdot\mathbf{H}/H^2\,\det\mathbf{m}_s.\quad(13)$$

The spin and orbital effective masses used are those at the bottom of the band. The masses on the Fermi surface are related to the bottom-of-the-band masses by

$$\mathbf{m}^*(E_F)=(1+2E_F/E_G)\mathbf{m}_b{}^*.\quad(14)$$

The carrier density per ellipsoid filled to energy E is given by

$$N(E)=\frac{2^{3/2}eH}{h^2c}(m_z)^{1/2}\sum_{n,s}[E^*-E(n,s)]^{1/2},\quad(15)$$

where

$$E^*=E(1+E/E_G)\,,\quad(16)$$

and

$$E(n,s)=(n+\tfrac{1}{2})\hbar\omega_c+\tfrac{1}{2}s\beta_0gH\,.\quad(17)$$

The sum is over values of n and $s=\pm1$ such that the radicand is positive. The density of states at the Fermi surface is given by

$$\eta(E_F)=[dN(E)/dE]_{E=E_F}.\quad(18)$$

Charge neutrality requires that

$$\sum_{i=1}^{3}N_i{}^e(E_F)=N^h(E_F)\,,\quad(19)$$

which states that the total number of electrons equals the total number of holes. We use Eq. (19) to determine the Fermi energy. First the value of the Fermi energy is guessed and Eqs. (15)–(17) are used to determine the number of holes and electrons. The value of E_F is then changed until the equality given by Eq. (19) holds.

Once the Fermi energy is obtained, Eqs. (15) and (18) give the number of carriers per ellipsoid and the density of states. The Alfvén-wave measurements give the mass density. The Alfvén-wave mass density $f(nm_e{}^*+pm_h{}^*)$, as defined in Sec. II, can be written in terms of the same expression evaluated using the bottom-of-the-band masses:

$$f(nm_e{}^*+pm_h{}^*)=(1+2E_F/E_G)f(nm_e{}^*+pm_h{}^*)_b.\quad(20)$$

Equation (20) shows explicitly the oscillatory dependence of the mass density, both through changes in the number of carriers n and p and changes in E_F.

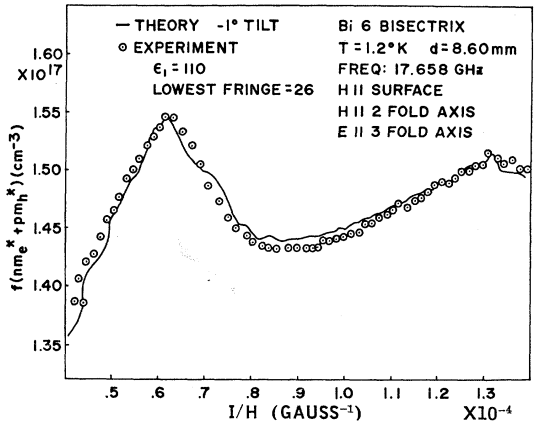

FIG. 2. Plot of experimental and theoretical mass-density versus inverse magnetic field for the magnetic field along the binary axis and the microwave electric field along the trigonal axis.

III. EXPERIMENTAL

The experimental details have been described elsewhere.[1,7,16] The magnetic field in these experiments was always parallel to the sample surface and perpendicular to the direction of microwave propagation. The frequency range used was from 12 to 18 GHz. The sample thicknesses ranged from 1 to 9 mm. The transmitted Alfvén-wave intensity exhibited a series of maxima and minima, a fringe pattern, as shown in Ref. 16. In these experiments all fringe patterns were of the leakage type.[7,16]

The intensity maxima are given by

$$N=d\epsilon^{1/2}/\lambda_0=dkc/\lambda_0\omega\,,\quad(21)$$

where d is the sample thickness, λ_0 is the free-space wavelength of the microwave radiation and N is the fringe index. Using Eq. (6) with $p-n=0$ in Eq. (21), we obtain

$$N=(d/\lambda_0)[\epsilon_l+4\pi m_0c^2f(nm_e{}^*+pm_h{}^*)/H^2]^{1/2}.\quad(22)$$

$f(nm_e{}^*+pm_h{}^*)$ represents the mass-density function for the anisotropic case. Except for very high fields, ϵ_l is small compared to the Alfvén-wave term. If we plot N versus $1/H$ we will expect a straight line whose slope is proportional to the mass density, $f(nm_e{}^*+pm_h{}^*)$. For evaluating the Alfvén-wave mass density, we are interested only in this slope. The absolute value of N is not required. Any value can be assigned to the highest field maximum. The remaining maxima are numbered in increasing sequence, corresponding to the fact that each fringe or maximum represents an additional full wavelength thickness for the sample.

When the data are plotted versus $1/H$ and a least-squares straight line is fitted, there appears a periodic

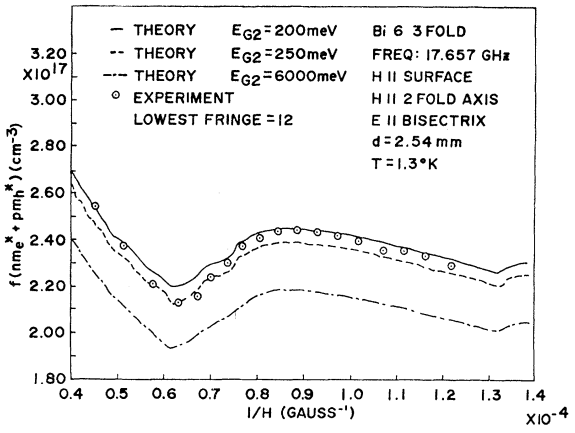

FIG. 3. Plot of experimental and theoretical mass-density versus inverse magnetic field for the magnetic field along the binary axis and the microwave electric field along the bisectrix axis. The three theoretical curves represent three values of E_{G2} as discussed in the text.

deviation from the straight-line behavior predicted by Eq. (22). This deviation is due to the Fermi energy oscillation as reported by Williams and Smith[1] and Williams.[7] In order to facilitate comparison with theory, it is convenient to change Eq. (22) to

$$f(nm_e^*+pm_h^*)=(\lambda_0^2N^2/d^2-\epsilon_l)H^2/4\pi m_0c^2. \quad (23)$$

If $\epsilon_l=100$, then at 20 kG the neglect of ϵ_l would introduce an error of about 5% in the value obtained for $f(nm_e^*+pm_h^*)$.

In order to use Eq. (23) the absolute value of N must be known. If experimental data at several frequencies on the same sample is available, it is possible to make some estimate for what this value should be. If a maximum occurs at some magnetic field value at a specific frequency, then there is an integral number of wavelengths in the sample. If the frequency is increased, more wavelengths may be accommodated in the sample. This results in a larger fringe index value. If two intensity maxima at different frequencies occur at the same magnetic field, then the fringe indices must be in the same ratio as the frequencies.[1] This limits the choice for N, but does not give a unique value.

There is another way to obtain N. Using Eq. (23) we pick various values for N and compute the resulting $f(nm_e^*+pm_h^*)$ versus $1/H$. For the proper choice of N the low-field portion of the curve will be flat. If N is too small, the curve will slope down. If N is too large, the curve will slope up. If the value of N chosen is very far from the correct value, the curves will appear nearly smooth because the periodic variation is wiped out. The above procedure gives the correct fringe index to approximately plus or minus one fringe index. The final determination is made in terms of the best fit to the theoretical curves. A check of this best fit can be made in the following manner: The maxima in the intensity fringes occur very nearly at $\cos(\omega d/V)=+1$, where V is the Alfvén-wave phase velocity, and

$$V=H[4\pi m_0 n f(m^*)]^{1/2}.$$

This gives the condition

$$N=\frac{\omega d[4\pi m_0 f(nm_e^*+pm_h^*)]^{1/2}}{2\pi H}. \quad (24)$$

The experimental data are plotted according to Eq. (23). The theoretical values for $f(nm_e^*+pm_h^*)$ are obtained by finding the number of carriers and Fermi energy at a certain magnetic field from Eqs. (15)–(19) and substituting these values into Eq. (20). [Bottom-of-the-band masses are found using the zero-field top-of-the-band masses chosen and the values of E_F and E_G chosen in Eq. (20).] We use the values of Smith, Baraff, and Rowell[2] for the g-spin effective-mass tensor. This means that in the theoretical expression we use as variables: the number of carriers n and p; the top-of-the-

TABLE I. Summary of parameters used to fit the experimental Alfvén-wave mass-density oscillations.

Effective masses (m_0 as unit)		
	Bottom of band	Top of band
m_1	0.00139	0.00651
m_2	0.291	1.362
m_3	0.0071	0.0297
m_4	±0.0359	±0.1635
M_1	0.059	0.0644
M_3	0.634	0.696
Energy-band parameters		
E_{G1}	15.0×10^{-3} eV	
E_F	$(26.6\pm0.18)\times10^{-3}$ eV	
E_0	$(38.2\pm0.15)\times10^{-3}$ eV	
E_{G2}	$(250\pm50)\times10^{-3}$ eV	
n	$(2.92\pm0.05)\times10^{17}$ cm^{-3}	

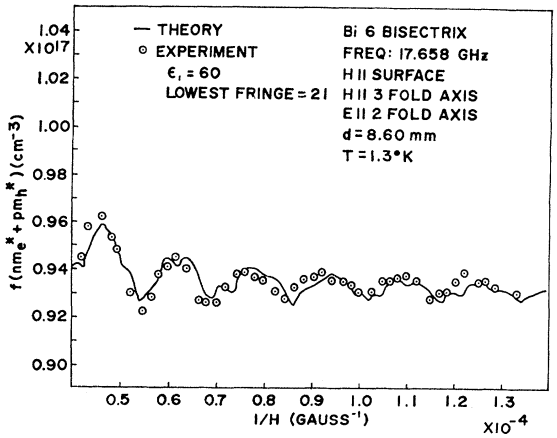

FIG. 4. Plot of experimental and theoretical mass-density versus inverse magnetic field for the magnetic field along the trigonal axis and the microwave electric field along the binary axis.

band masses for the electrons and holes m_1, m_2, m_3, m_4, M_1, and M_3; the energy gaps E_{G1} and E_{G2}; and the overlap energy E_0. The values of n and the masses are taken from the range of values given by the Alfvén-wave mass-density results.[16] We chose the gap energy E_{G1} to be 15 meV.[28] The value of the overlap has been reported to be between 36 [28] and 38.5 meV.[2] Therefore, we attempted to fit the experimental data so that the overlap energy falls in this range. The value of the second energy gap E_{G2} is less well known. Estimates have varied from 100 [21,22] to about 700 meV.[27] As a first approximation, we attempted to fit the experimental data with a very large value of E_{G2} (6000 meV), a large value of E_{G2} indicating that band 4 has very little influence on band 2. We then varied E_{G2} to smaller values to improve the fit.

IV. RESULTS AND DISCUSSION

In order to fit the theoretical curves to the experimental ones, as given in Figs. 2–6, we began with the masses and number of carriers reported by Isaacson and Williams.[16] The masses and number of carriers shown in Table I were arrived at by fitting theory to experiment for the data in Figs. 2 and 3. The theory curves in Figs. 4–6 were then calculated using these parameters with no further adjustment. The values of the parameters given in Table I are within the range specified in Ref. 16. This work can thus be viewed as a refinement of the values of Ref. 16.

By adjusting the masses we were able to make the peak of the theoretical curves occur at the same magnetic field as the peaks of the experimental data, Fig. 2. When this was accomplished, the theoretical and experimental results still did not agree. The experimental points were rotated with respect to the theoretical curves. That is, high-field experimental points were too high. Two things can cause this. The first is the use of an incorrect value for the absolute fringe index. The second is the neglect of ϵ_l. Neglecting ϵ_l causes the high-field experimental points to have too large an Alfvén-wave mass density. Incorrect values of the fringe index causes the theoretical curve to deviate from the experimental curve at all fields. To be assured that the correct value of fringe index is used, the difference in the peak values of the mass density of the theoretical curve, at inverse magnetic fields of 0.62×10^{-4} and 1.32×10^{-4} G^{-1}, was required to be the same as the difference in the experimental values at the same fields, Fig. 2. If the chosen experimental fringe index value is not correct, these differences do not agree. The procedure described in Sec. III produces a value of fringe index within plus or minus one of the true value. Once the correct value for the fringe index is found, the remaining rotation of the experimental and theoretical curves must be due to the neglect of ϵ_l. In Fig. 2, we used a value of ϵ_l equal to 110 in order to fit the experimental data.

The orientation shown in Fig. 2 is not sensitive to E_{G2} values, but the orientation of Fig. 3 is sensitive to E_{G2}. This occurs because the mass density for Fig. 2 is dominated by electron-mass components, and the mass density for the orientation in Fig. 3 is dominated by a hole mass component.[7,16] The value of E_{G2} necessary to fit the experimental points in Fig. 3 is between 200 and

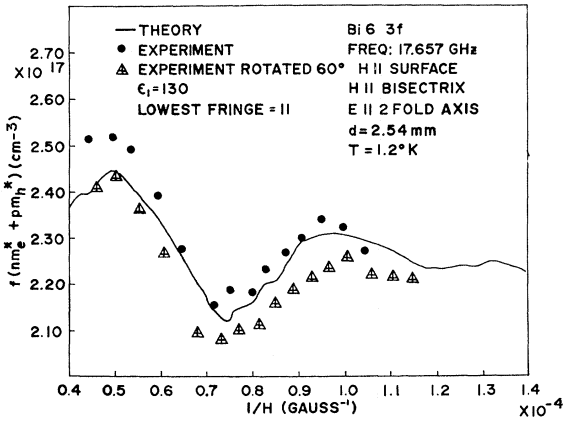

FIG. 5. Plot of experimental and theoretical mass density versus inverse magnetic field for the magnetic field along the bisectrix axis and the microwave electric field along the binary axis. The triangles represent the results when the magnetic field was rotated 60° around the threefold axis. From the symmetry of the crystal, the data represented by the circles and triangles should be identical. That they are not precisely identical is an indication of minor sample misalignment.

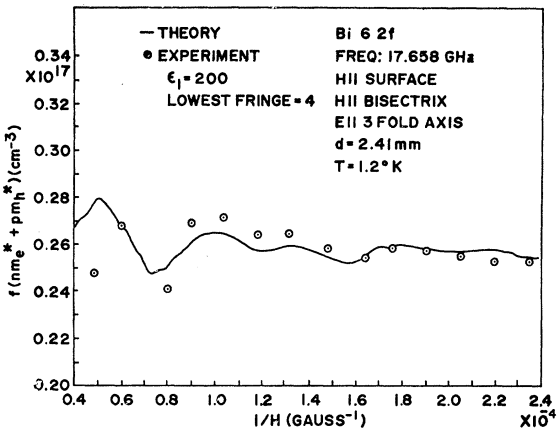

FIG. 6. Plot of experimental and theoretical mass-density versus inverse magnetic field for the magnetic field along the bisectrix axis and the microwave electric field along the trigonal axis.

TABLE II. Values of lattice dielectric constant needed to fit the experimental data.

H‖axis	E‖axis	Lattice dielectric constant
1	2	any value less than 200
1	3	90–150
2	1	70–130
2	3	150–200
3	1	40–80

250 meV. Values of gap energy larger than 250 meV used with the parameters from the fit of Fig. 2 produce theoretical mass densities that are too low. Values of gap energy lower than 200 meV distort the shape of the theoretical results too much to agree with the experimental shape. Figures 4–6 show the comparison of theory and experiment using the parameters of Table I that are deduced from the theory-experiment fit shown in Figs. 2 and 3. Our values for E_{G2} are in agreement with the tunneling results of Hauser and Testradi.[32] They find a conductance maximum at 200 meV with respect to the Fermi level. This value corresponds to an E_{G2} of 188 meV on our model.

A value for E_{G2} in the energy region 200–250 meV should cause the hole band to be slightly nonparabolic. If E_{G2} were less than 200 meV the hole band should be markedly nonparabolic. Previous experimental evidence[21–23] indicates that the hole band is only slightly nonparabolic.

A gap as small as 100 meV is not consistent with the Alfvén-wave results. Antcliffe and Bate[21] have reported evidence, from Shubnikov–de Haas measurements, of higher bands at 55 and 73 meV. These results are obtained with bismuth-tellurium alloys. Their results are not necessarily at variance with those reported here. We have assumed a particular form and location in k space for band 4. This form may represent the effect of other bands located elsewhere in k space. Bate and Einspruch[22] reported a value of 66 ± 25 meV for the gap contributing to the hole-band nonparabolicity, using galvanomagnetic data. This is definitely in disagreement with the gap reported in this work.

It is apparent from Table II that ϵ_l depends on crystal orientation. There are two contributions to the spread of values for ϵ_l reported here. There is a certain insensitivity to the values of ϵ_l used especially in the low-field region. The larger the Alfvén-wave mass density the less effect ϵ_l has. In any case the effect of ϵ_l increases with increasing field. In addition, in several orientations one value of ϵ_l fits most of the data but a higher value of ϵ_l is needed to fit the high-field points. The change is not large. This variation indicates there may be a magnetic field dependence to ϵ_l. High-field results for ϵ_l will be reported at a later date. Boyle and Brailsford[33] report a value of 100 for the lattice dielectric constant. This is for the case of magnetic field parallel to the direction of propagation and parallel to the trigonal axis. Our results are for magnetic field perpendicular to the direction of propagation. The value of 100 could be considered as a mean value of our results.

The dielectric constant ϵ_l consists of a part due to the background lattice and a part due to the zero-frequency polarizability of the electron gas. It is this zero-frequency polarizability that is important. There are conduction and valence bands in bismuth with very small energy separation. These neighboring bands give rise to virtual electron transitions in the far-infrared frequency region. Wolff[34] points out that a large value of ϵ_l requires both a small energy gap between conduction and valence bands and highly anisotropic masses. Wolff presents an expression for the qualitative behavior of ϵ_l showing it to be a tensor depending on the mass tensor. Hence, the fact that ϵ_l depends on crystallographic direction is not surprising. It should also not be surprising if ϵ_l has some dependence on magnetic field, since at large magnetic fields the energy gap may beome field-dependent.[35,36]

V. SUMMARY

In summary, we have measured the quantum oscillations of the mass density along principal crystal direction in bismuth and compared these results to the theoretical model of the bismuth Fermi surface. In contrast to Williams and Smith,[1] we find a good fit between experiment and theory for all orientations of the magnetic and electric field with respect to the crystal axes. Inspection of their Figs. 11 and 12 and comparison with the data reported here lead to the conclusion that the experimental data of Williams and Smith is mislabeled, and the experimental points for Figs. 11 and 12 of their paper should be interchanged. In their work, Figs. 11 and 12 represent consecutive experiments in which only the plane of polarization of the microwaves was changed. One of us (G. W.) concedes that an error probably occurred in assigning the data to particular orientations.

A simple three-band model used by Smith, Baraff, and Rowell[2] is sufficient to account for the general shape of the experimental curves. The extra conduction band, band 4 in Fig. 1, is needed to make a detailed fit of the experimental curves. Within experimental error it has not been necessary to postulate any nonellipsoidal character to the Fermi surfaces, but this cannot be ruled out by these experiments.

The results of the fit of experiment and theory indicate that ϵ_l is anisotropic and is of the order of magnitude of 100.

ACKNOWLEDGMENTS

The authors wish to thank E. H. Hygh for a critical reading of the manuscript, and G. E. Smith for providing the computer program, which was used in a somewhat modified form.

[32] J. J. Hauser and L. R. Testradi, Phys. Rev. Letters **20**, 12 (1968).
[33] W. S. Boyle and A. D. Brailsford, Phys. Rev. **120**, 1943 (1960).
[34] P. A. Wolff (unpublished).
[35] G. A. Baraff, Phys. Rev. **137**, A842 (1963).
[36] S. Takano and H. Kawamura, Phys. Letters **26A**, 187 (1968).